# Solution-Processed Highly Efficient Alternating Current-Driven Field-Induced Polymer Electroluminescent Devices Employing High-*k* Relaxor Ferroelectric Polymer Dielectric

*Yonghua Chen, Yingdong Xia, Hengda Sun, Gregory M. Smith, Dezhi Yang, Dongge Ma,* and David L. Carroll**

**Organic thin-film electroluminescent (EL) devices, such as organic light-emitting diodes (OLEDs), typically operate using constant voltage or direct current (DC) power sources. Such approaches require power converters (introducing power losses) and make devices sensitive to dimensional variations that lead to run away currents at imperfections. Devices driven by time-dependent voltages or alternating current (AC) may offer an alternative to standard OLED technologies. However, very little is known about how this might translate into overall performance of such devices. Here, a solution-processed route to creating highly efficient AC field-induced polymer EL (FIPEL) devices is demonstrated. Such solution-processed FIPEL devices show maximum luminance, current efficiency, and power efficiency of 3000 cd $m^{-2}$, 15.8 cd $A^{-1}$, and 3.1 lm $W^{-1}$ for blue emission, 13 800 cd $m^{-2}$, 76.4 cd $A^{-1}$, and 17.1 lm $W^{-1}$ for green emission, and 1600 cd $m^{-2}$, 8.8 cd $A^{-1}$, and 1.8 lm $W^{-1}$ for orange-red emission. The high luminance and efficiency, and solution process pave the way to industrial roll-to-roll manufacturing of solid state lighting and display.**

## 1. Introduction

Organic thin-film electroluminescent (EL) devices are currently under intensive research and development worldwide as a next generation light source to replace problematic incandescent bulbs and fluorescent tubes. Organic EL devices, however, typically operate with direct current (DC) voltage, for example, organic light-emitting diodes (OLEDs),[1] which necessitated costly switching mechanisms built into such products in turn, introducing power losses and in addition complicated back end electronics. Recently, light emission from AC electric field activation of organic small molecules or conjugated polymers has gained significant attention as a potential alternative to standard OLED technologies.[2–11] These devices driven by AC consist of thin organic films placed on/below a dielectric layer or sandwiched between dielectric layers.[4,5] Light generation is achieved through the AC field-induced creation of excitons-bipolar charges injected from an electrode[3,4,8–11] or generated in the internal charge generation layers, and the subsequent recombination of these holes and electrons in the emissive layer (EML).[2,5–7] Due to frequent reversal of the applied voltage, AC driven EL devices avoids the charge accumulation in the device,[5] which may reduce the triplet–triplet or triplet–charge annihilation in the phosphorescent devices' operation. Moreover, the dielectric layer can effectively prevent electro-chemical reactions between the organic layer and the electrodes and protecting from degradation due to external moisture and oxygen in the atmosphere.[4] Most recently, we found that the usual concentration dependence of emission from the dye is not observed in a hybrid system comprising of a blue fluorophor and a red phosphor dye, due to the unique carrier injection characteristics of the field-induced device.[10] This further suggests that greater color tunability may be found in such devices as compared to typical OLED structures.

To realize high-efficiency AC field-induced EL devices, two major factors have to be taken into account. First, excitons must be efficiently created to increase the light intensity.[4,5,9,11] Second, the dielectric constant of insulating layers must be high to improve the breakdown voltage and lower the driving voltage.[6,7] To efficiently create excitons, Tsutsui et al.[2] reported that metal nanoparticles were embedded between the emitter and the dielectrics in an attempt to increase charge generation, bright surface emission of 81 cd $m^{-2}$ was observed. Moreover, single-walled carbon nanotubes (SWNTs) were dispersed into EML by Park and co-workers to facilitate the bipolar charge injection,[4,8] a higher brightness of 350 cd $m^{-2}$ was achieved. Recently, 27.5 times improvement in luminance has been reported by our work,[11] where device exhibits 550 cd $m^{-2}$ by electrode modification with calcium (Ca/Al. Moreover, Perumal et al.[5–7] employed the concept of molecular doping for small molecule organic semiconductors, allowing for the efficient generation

Dr. Y. Chen, Dr. Y. Xia, G. M. Smith, Prof. D. L. Carroll
Center for Nanotechnology and Molecular Materials
Department of Physics
Wake Forest University
Winston-Salem, NC 27105, USA
E-mail: carroldl@wfu.edu
H. Sun, Dr. D. Yang, Prof. D. Ma
State Key Laboratory of Polymer Physics and Chemistry
Changchun Institute of Applied Chemistry
Chinese Academy of Sciences
Changchun 130022, P. R. China
E-mail: mdg1014@ciac.jl.cn

**DOI: 10.1002/adfm.201302587**

of charge carriers and for the charge transport. A luminance of up to 1000 cd $m^{-2}$ was obtained. For the dielectrics, the polymer dielectrics are easy to process in solution, but the dielectric constant of common polymer dielectrics including polystyrene (PS, $k \approx 2.6$), poly(methyl methacrylate) (PMMA, $k \approx 3.5$), and poly(vinyl phenol) (PVP, $k \approx 4.2$) are very low.[12] The inorganic dielectrics, for example, silicon dioxide ($SiO_2$, $k \approx 4.5$)[4,5,8] and hafnium dioxide ($HfO_2$, $k \approx 21$),[6,7] provide an alternative due to their higher dielectric constant and better chemical stability. The turn-on voltage can be significantly lowered and the luminance was remarkably improved using high-$k$ $HfO_2$ dielectric layers in state-of-the-art AC field-induced devices.[6,7] The small molecular emitters associated with charge generation layers reach maximum brightness levels of 1500 cd $m^{-2}$ and 5000 cd $m^{-2}$ with optical design.[6,7] However, the high temperature sputtering of inorganic dielectric layer on top of organic films limits the combination with the delicate organic molecules, resulting in potential reducing the device stability. Most importantly, the power efficiency in such AC-driven EL devices which is very important parameter for a light-emitting device is typical lower than 1 lm $W^{-1}$.[5,6] Although enhancing the efficiency up to 2.7 lm $W^{-1}$ by optimizing the operation frequency has been reported,[7] it still limits its practical application in solid state lighting and display. One feasible method to overcome this drawback is to find a much higher dielectric constant ($k$) dielectric to use in the devices.

One interesting relaxor ferroelectric polymer poly(vinylidene fluoride-trifluoroethylene-chlorofluoroethylene) [P(VDF-TrFE-CFE)] has recently attracted much attention due to its application in energy storage, actuators, and nonvolatile memory.[13–15] P(VDF-TrFE-CFE) also exhibits excellent dielectric properties and shows high-$k$ values at room temperature,[14] which has successfully been used in low-voltage top-gate organic thin film transistors based on many high mobility semiconducting polymers.[16] Moreover, the P(VDF-TrFE-CFE) is solution processable, uniform, and have high electric strength. Therefore, P(VDF-TrFE-CFE) is a good candidate for the dielectric of low-voltage, solution processable, and high-efficiency AC field-induced EL devices, which have never been reported before.

Here, we present a new paradigm for highly efficient AC field-induced polymer EL (FIPEL) devices that is solution-processed (**Figure 1**a). The key feature of our strategy is employing a solution processable high-$k$ P(VDF-TrFE-CFE), a solution processable thermally polymerizable polymer poly(*N*,*N*′-bis(4-butylphenyl)-*N*,*N*′-bis(phenyl)benzidine) (Poly-TPD)[17] doped tetrafluoro-tetracyano-quinodimethane (F4TCNQ) as the hole generation layer (HGL),[18] and a solution processable high-triplet and high-electron-mobility material 1,3,5-tri(m-pyrid-3-yl-phenyl)benzene (TmPyPB) as the electron transporting layer (ETL)[19] (Figure 1a). The devices have maximum luminance values of 3000 cd $m^{-2}$, 13 800 cd $m^{-2}$, and 1600 cd $m^{-2}$ for blue, green, and orange-red emission, respectively, without any outcoupling technology and optical design, which are the highest values of luminance reported to date. Moreover, due to the high-$k$ P(VDF-TrFE-CFE) dielectric Poly-TPD:F4TCNQ HGL and TmPyPB ETL allows the efficient hole generation in HGL and electron transport in ETL (Figure 1b), demonstrating improved current efficiency ($\eta_{cd}$) and power efficiency ($\eta_p$). The maximum $\eta_{cd}$ and $\eta_p$ were 15.8 cd $A^{-1}$, and 3.1 lm $W^{-1}$ for blue, 76.4 cd $A^{-1}$, and 17.1 lm $W^{-1}$ for green, and 8.8 cd $A^{-1}$, and 1.8 lm $W^{-1}$ for orange-red emitting devices, respectively.

## 2. Results and Discussions

The terpolymer P(VDF-TrFE-CFE) 62.6/29.4/8 mol% dielectric film shows uniform thickness by Atomic force microscopy (AFM) (Supporting Information, Figure S1). The microstructure is also presented by scan electron microscope (SEM) and shown in **Figure 2**a, where the presence of the amorphous phase and random orientations of the polymer chanis can be estimated.[20] Moreover, the phase structure of the P(VDF-TrFE-CFE) film was examined using wide-angle X-ray diffraction (XRD) (Figure 2b). The (110, 200) reflection is at $2\theta = 18.58°$, indicating an interchain spacing of 4.77 Å, which corresponds to the previous report[20] and confirms its intrinsic semicrystalline nature.[21] Figure 2c shows the $k$ value of the P(VDF-TrFE-CFE) terpolymer as a function of measurement frequency at room temperature. The $k$ value is as high as 65 in a low frequency range (10 kHz). At high frequencies up to 100 kHz, the $k$ value is higher than 46, which is much higher than that of common polymer dielectrics.[12] The high $k$ value of the P(VDF-TrFE-CFE) terpolymer originates from the strong C-F dipoles and their strong correlation in this relaxor ferroelectric polymer.[22] Due to the dielectric properties of the P(VDF-TrFE-CFE) terpolymer, it can meet the requirements of the FIPEL devices which generally operate from low to high frequency. For the device fabrication, a big challenge for the solution-processed multilayer structure is that the orthogonal solvents are needed to avoid compromising the integrity of the underlying layers while depositing overlayers. In our work, however, it should be noted that the Poly-TPD:F4TCNQ HGL and the subsequent EML are both dissolved in chlorobenzene spin-coated for the device fabrication. A cross-sectional SEM image of the FIPEL device is shown in Figure 2d. The distinct interface between Poly-TPD:F4TCNQ HGL and EML indicates that the Poly-TPD:F4TCNQ HGL was not contaminated by the top EML in the device fabrication, which can be attributed to the thermally polymerizable characteristics of Poly-TPD.[17]

**Figure 3**a shows the luminance characteristics as a function of driving voltage ($L$–$V$) characteristics of FIPEL devices with different EMLs. The luminance intensity was gradually increased by incrementing the driving voltage in all devices at a fixed frequency of 60 kHz since higher AC currents are flowing in the all FIPEL devices at higher driving voltages (Supporting Information, Figure S2).[11] The maximum luminance for the blue, green, and orange-red devices was 3000, 13 800, and 1600 cd $m^{-2}$, respectively. These values are a factor of 3–9 higher than previously reported highest luminance from AC EL devices.[2–11] This strongly suggests that holes can be effectively generated and transported in the Poly-TPD:F4TCNQ HGL and electrons were efficiently injected into the EML followed by formation of excitons at the interface between EML and TmPyPB ETL at AC driving voltages. According to the schematic energy level diagram shown in Figure 1b, the effective charge transfer from Poly-TPD to F4TCNQ can be occurred, which was verified by the photoluminescence (PL) quench (Supporting Information, Figure S3), and more holes are available with

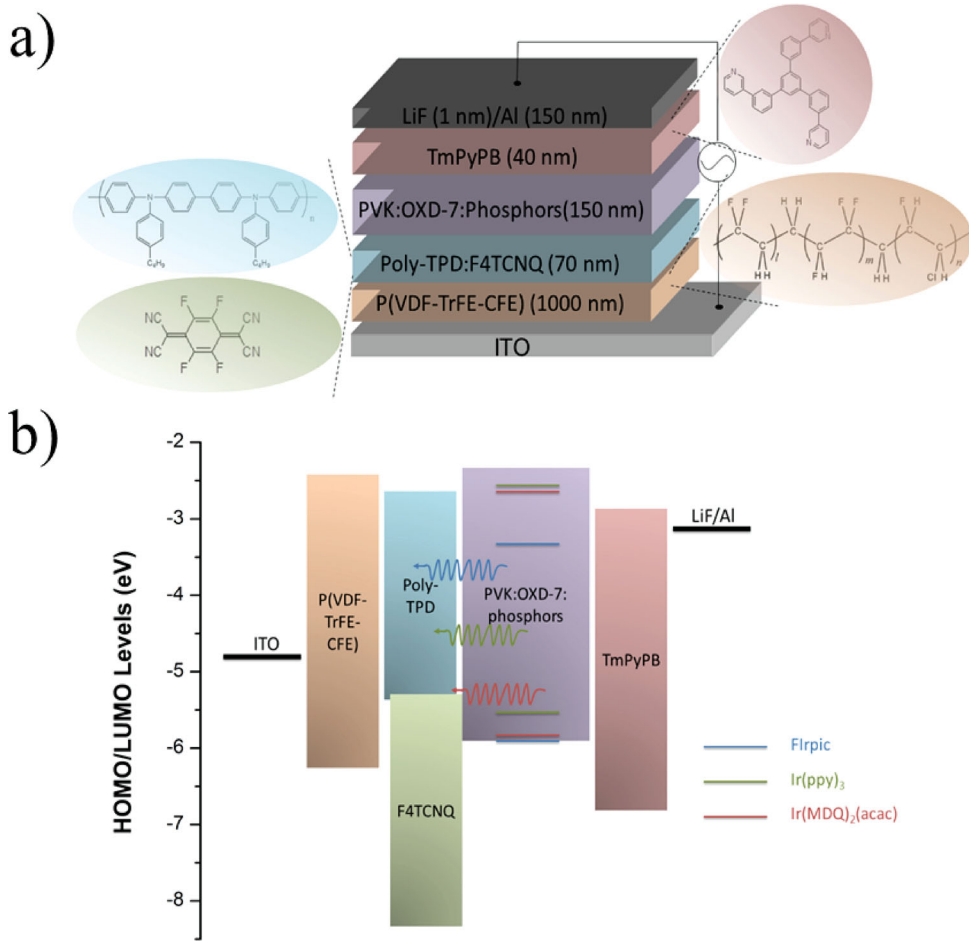


**Figure 1.** Device structure and energy levels of the solution-processed FIPEL devices. a) Schematic of the FIPEL device structure, in which a dielectric layer P(VDF-TrFE-CFE) placed against the bottom indium tin oxide (ITO) electrode and the EML is sandwiched between a HGL, Poly-TPD:F4TCNQ and an ETL, TmPyPB. The EML consisted of poly (*N*-vinylcarbazole) (PVK):1,3-bis(2-(4-*tert*-butylphenyl)-1,3,4-oxadiazo-5-yl)benzene (OXD-7):bis(3,5-difluoro-2-(2-pyridyl) phenyl-(2-carboxypyridyl)iridium (FIrpic) for blue, PVK:OXD-7:fac-tris(2-phenylpyri-dine)iridium(III) [Ir(ppy)$_3$. for green, PVK:OXD-7:bis(2-methyldibenzo[f,h]quinoxaline) (acetylacetonate) iridium (III) [Ir(MDQ)$_2$(acac)) for orange-red. The final device structure is: ITO/P(VDF-TrFE-CFE) (1000 nm)/Poly-TPD:F4TCNQ (7%, 70 nm)/EML (150 nm)/TmPyPB (40 nm)/LiF (1 nm)/Al (150 nm). Insets: chemical structures of the materials used in the study. b) Schematic energy-level diagram for the various layers of the optimized FIPEL device.

increasing the concentration of F4TCNQ (Supporting Information, Figure S4). Note that although the hole generation capability in Poly-TPD:F4TCNQ HGL is improved with increasing the concentration of F4TCNQ, the FIPEL devices achieves the maximum luminance at 7% F4TCNQ doped Poly-TPD due to the limited solubility of F4TCNQ (Supporting Information, Figure S5). Moreover, with a lowest unoccupied molecular orbital (LUMO) of 2.7 eV and a highest occupied molecular orbital (HOMO) of 6.8 eV the TmPyPB ETL not only provides efficient electron injection from the LiF/Al cathode into EML, but also helps to confine holes within the EML layer due to the HOMO offset at the EML/TmPyPB interface,[23] leading to an improved charge recombination efficiency. The high triplet of TmPyPB (2.78 eV) also effectively avoids the exothermic triplet energy transfer from phosphors to TmPyPB,[23] confining the excitons in the EML and thus remarkably improving the utilization of excitons. The poor device performances are consequently inevitable without either layer (Supporting Information, Figure S6). It is necessary to determine if the voltage in the devices were beyond the breakdown voltage. DC test, therefore, was made on the green emitting device and no luminance was observed in this case. The currents measured in the device are very low ($8 \times 10^{-5}$ mA, Supporting Information, Figure S7). This is obvious from the capacitive nature of the device.

The luminance characteristics as a function of frequency (*L–f*) characteristics for fixed AC-driven electric fields for all FIPEL devices are plotted in Figure 3b. The light emission is frequency dependent in our devices. The luminance output from all devices increased as the frequency increased, but the luminance decreases after 60 kHz.[11] However, the increase in luminance as a function of frequency is not merely due to increase in light emitting cycles. From low to high frequency, the increase in luminance beyond a threshold frequency is due to the increase in current flowing through the device since the capacitive reactance of the device is inversely proportional to the frequency. Although the capacitive reactance of the device

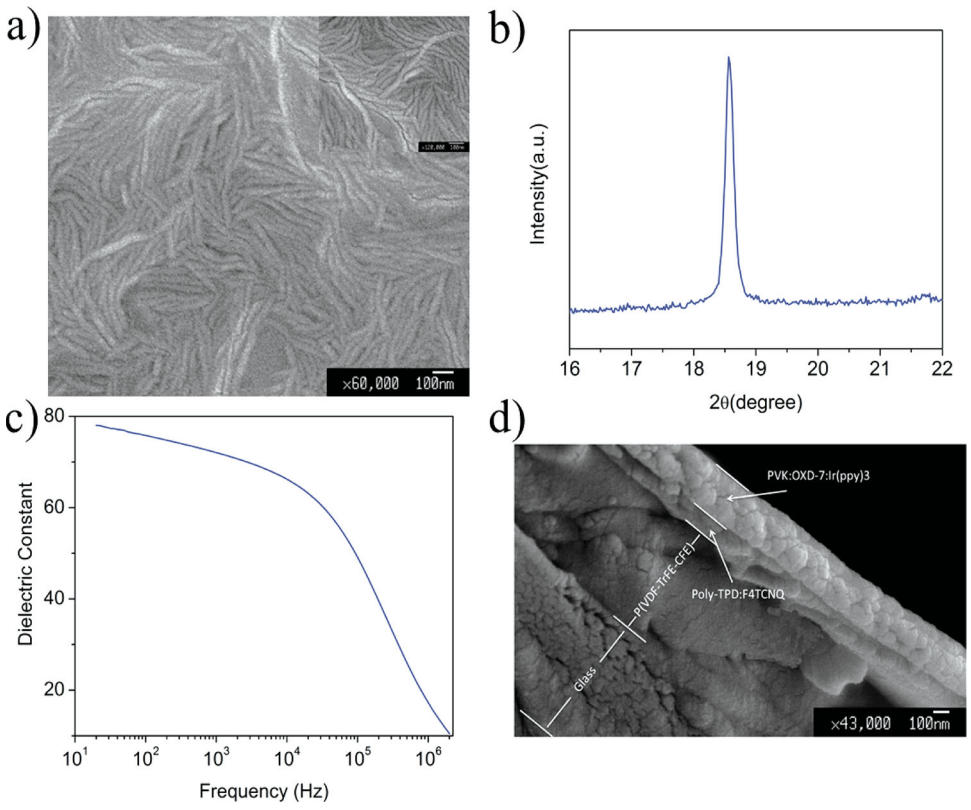


**Figure 2.** The morphology and dielectric characteristics of P(VDFTrFECFE) terpolymer, and the interface characteristics between HGL and EML in solution-processed fabrication. a) SEM image and b) XRD patterns for the (110, 200) of P(VDFTrFECFE) 62.6/29.4/8 mol% trepolymer. c) *k* values (dielectric constant) of P(VDFTrFECFE) film as functions of measurement frequency from 20 Hz to 2 MHz at room temperature. d) The cross-sectional SEM image of a sample with Glass/P(VDFTrFECFE)/Poly-TPD:F4TCNQ/PVK:OXD-7:Ir(ppy)$_3$.The interface between Poly-TPD:F4TCNQ and PVK:OXD-7:Ir(ppy)$_3$ is observed to be continuous one.

decreases, however, the charge carrier recombination begins to be limited by mobility of organic materials, which leads to a decrease in the luminance beyond a particular frequency (60 kHz). It is possible that the charge carriers appear to be static at very high frequencies,[5] that is, the electrons may not even be injected or the generated holes could not be extracted, resulting in a reduction of the number of charge carriers available in EML and thus decreasing the luminance. Note that the decrease of luminance as a function of the decreasing frequency (ultimately DC), clearly indicates again that the device does not respond to the DC voltage.[5]

Our FIPEL devices exhibit significantly enhanced device efficiency. It is first noteworthy that the FIPEL yields a nearly ideal Lambertian emission profile (Supporting Information, Figure S8) The $\eta_{cd}$ is defined as the ratio of luminance output from the device to the RMS current flowing the device, which is given in candela per ampere (cd $A^{-1}$). The $\eta_p$ is defined as the ratio of photometric power emitted from the device to the electrical input power, which is measured by inserting a series resistor to the device. This ratio is given in lumen per watt (lm $W^{-1}$). The power input per sample area is calculated as,[5]

$$P\left[\mathrm{W/m^2}\right] = \frac{1}{AT}\int_0^T V_{\mathrm{RMS}}(t)\, I_{\mathrm{RMS}}(t)\, \mathrm{d}t$$

$$P\left[\mathrm{W/m^2}\right] = \frac{1}{A}\, V_{\mathrm{RMS}}\, I_{\mathrm{RMS}}\, \cos(\varphi)$$

where $\varphi$ is the phase angle (in degrees, 83.7° at 60 kHz) between sinusoidal voltage and current. Then the $\eta_p$ is given by,

$$\eta_p\,[\mathrm{lm/W}] = \pi\, \frac{L\left[\mathrm{cd/m^2}\right]}{P\left[\mathrm{W/m^2}\right]}$$

Figures 3c,d show the $\eta_{cd}$ and $\eta_p$ of FIPEL devices as a function of luminance. The maximum $\eta_{cd}$ and $\eta_p$ of 15.8 cd $A^{-1}$ and 3.1 lm $W^{-1}$, 76.4 cd $A^{-1}$ and 17.1 lm $W^{-1}$, and 8.8 cd $A^{-1}$ and 1.8 lm $W^{-1}$ were achieved for the blue, green, and orange-red devices, respectively. The $\eta_{cd}$ are comparable with or even higher than solution-processed or evaporating small-molecular OLEDs and light-emitting transistors.[24–29] Moreover, the power efficiency of green device is even 6 times higher than the previous highest value report.[7] Note that the peak efficiencies of the current FIPEL devices are achieved at high luminance, which is different from OLEDs usually accompanied by efficiency roll-off at high luminance,[30,31] and more desired for practical display and lighting applications. The normalized EL spectra of the FIPEL devices were shown in Figure 3e. The triplet emission at peaks of 472 nm, 516 nm, and 590 nm are stemmed from FIrpic, Ir(ppy)$_3$, and Ir(MDQ)$_2$(acac), respectively, which corresponds to their PL

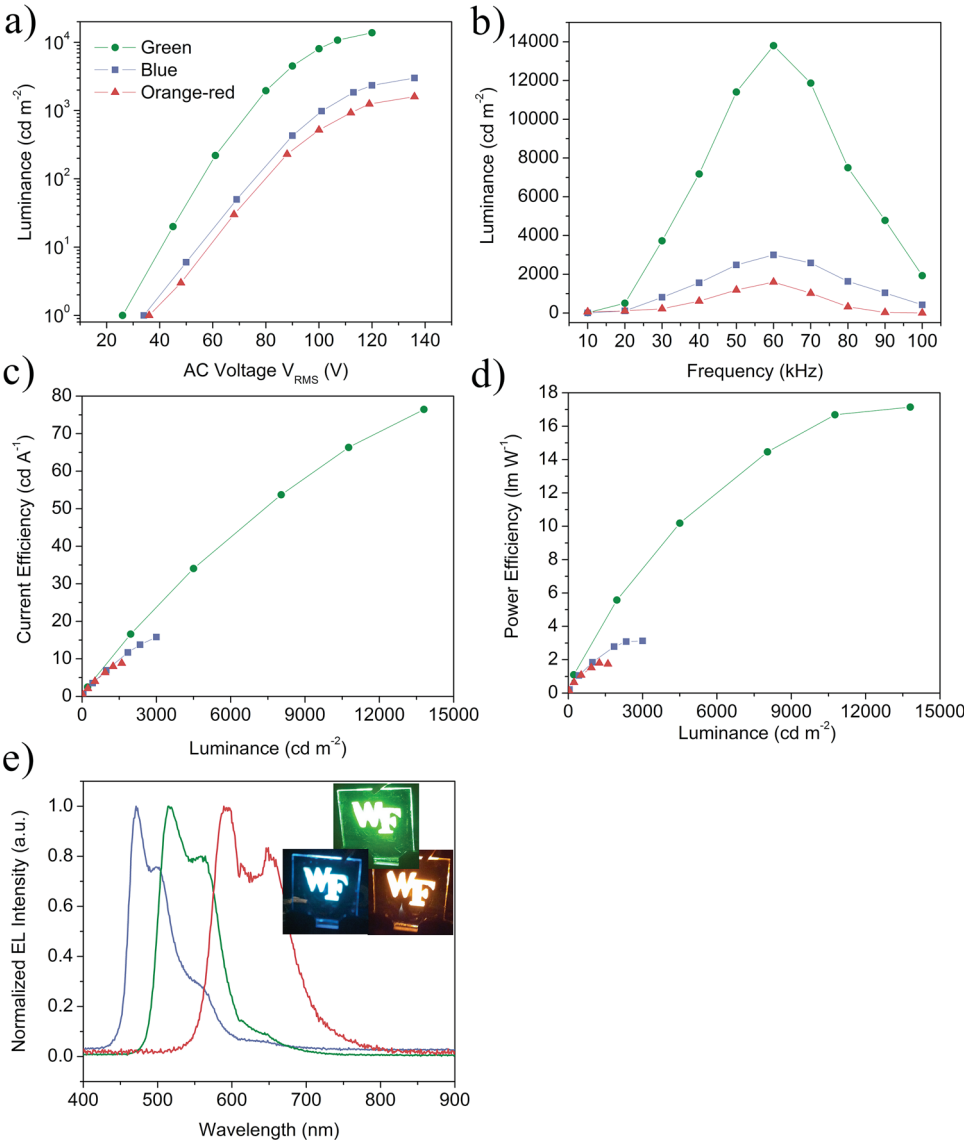


**Figure 3.** EL performances of solution-processed FIPEL devices with blue, green, and orange-red emission. a) Luminance-voltage (*L–V*) characteristics of the devices at a fixed frequency of 60 kHz. b) Luminance-frequency (*L–f*) characteristics of the devices at a fixed driving voltage of 136 V, 120 V, and 136 V for blue, green, and orange-red emitting devices, respectively. c) Current efficiencies characteristics as a function of luminance. d) Power efficiencies characteristics as a function of luminance. e) Normalized EL spectra and images of solution-processed FIPEL devices with peak emission wavelengths of 472 nm (blue), 516 nm (green), and 590 nm (orange-red).

spectra (see Supporting Information, Figure S9). The inset shows photographs of the three operating devices fabricated on 1 inch$^2$ substrates. **Table 1** summarizes the detailed performance parameters of the three different-colored FIPEL devices of the present study.

**Table 1.** Summary of the performance of the solution-processed FIPEL devices with blue, green, and orange-red emission. $L_{max}$ is the maximum luminance, $\eta_{cd,max}$ is the maximum current efficiency, and $\eta_{p,max}$ is the maximum power efficiency.

| Color | $L_{max}$ [cd m$^{-2}$] | $\eta_{cd,max}$ [cd A$^{-1}$] | $\eta_{p,max}$ [lm W$^{-1}$] | Peak Emission [nm] |
|---|---|---|---|---|
| Blue | 3,000 | 15.8 | 3.1 | 472 |
| Green | 13,800 | 76.4 | 17.1 | 516 |
| Orange-red | 1,600 | 8.8 | 1.8 | 590 |

For a capacitive AC driving device, impedance, resistance, reactance, and the phase angle are very important quantities. **Figure 4** shows impedance, resistance, reactance, and the phase angle as a function of frequency. All three resistive quantities show a pronounced decrease from low to high frequency, which correspond to the previous report,[7] whereas the phase angle only drops a little from 88° to 82° at this range of frequency. The decreased impedance and reactance with increasing frequencies further demonstrates that our FIPEL is a typical capacitive device.[7] As expected for a capacitive coupled device, the impedance is dominated by the reactance whereas a significantly smaller contribution comes from the resistance. The values can

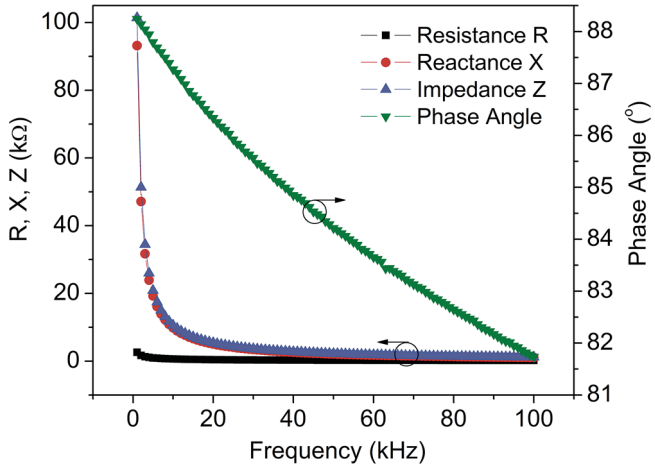


**Figure 4.** Capacitive characteristics of green FIPEL device. Resistance *R*, reactance *X*, impedance *Z*, and the phase angle as a function of frequency.

also be quantitatively understood and reasonable. Capacitive reactance *X*, for example, is inversely proportional to the frequency *f* and the capacitance *C*, which can be given by,

$$X = 1/2\pi fC$$

According to the values of frequency and capacitance of the FIPEL devices (Supporting Information, Figure S10), the calculated reactance is almost the same as the experimental one. The further studies on frequency dependence of light emission in greater detail are on the way.

The AC operation of the green FIPEL device is confirmed by the time-resolved EL (TREL) measurements to record the luminance time response of the device, which is measured at a constant frequency of 50 Hz and as a function of the applied square-pulsed voltage shown in **Figure 5**a. Although sinusoidal voltage was used in device operation, it can better describe the device operation mechanism based on the square-pulsed voltage in comparison to the sinusoidal voltage.[5] The luminance time response is similar in blue and orange-red devices. The TREL was observed only in the negative half of the AC cycle, where the applied AC field assists in the formation of excitons and light generation. We therefore propose the following mechanism for the charge generation and injection in the device. In the negative half of the AC cycle, as shown in Figure 5 b (left scheme), holes are generated in the Poly-TPD:F4TCNQ HGL and move towards to the interface of EML/TmPyPB under AC electric field while, simultaneously, electrons are injected into EML from LiF/Al electrode through TmPyPB ETL. The holes and electrons in the EML then form excitons that subsequently emit light upon recombination. As the doped transport layers provide only a limited amount of free charge carriers, a mechanism has to exist which regenerates charge carriers in Poly-TPD:F4TCNQ HGL layer. We can therefore conclude that the positive half of the AC cycle is essential for device operation although we did not observe any light emission from the device.

In contrast to a recent publication[5–7] where Zener-tunneling is suggested as a possible way to regenerate charge carriers, however, we already observe light emission at much lower voltages (Figure 3a) than the required for Zener-tunneling. We

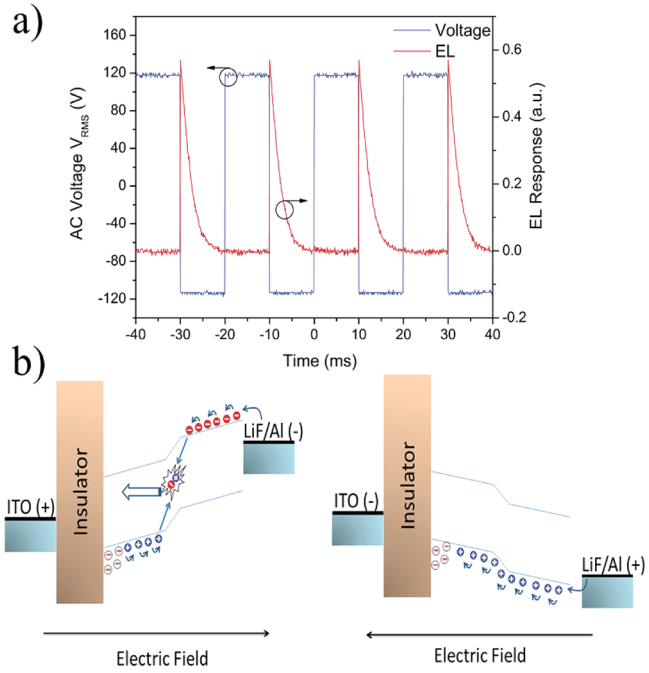


**Figure 5.** The time-resolved EL (TREL) measurements of the solution-processed FIPEL devices with green emission under square-pulsed alternating voltage trains and schematics of the proposed mechanism of device operation. a) The time-resolved alternating voltage pulse at 50 Hz (left axis) and the corresponding TREL as recorded by the photodetector (right axis). The device emits light only in the negative half of the AC cycle. b) Schematic of energy level alignment with the applied bias, shown for forward and reverse AC driving voltage. When a negative field is applied to device, holes are generated in the Poly-TPD:F4TCNQ HGL and move towards to the interface of EML/TmPyPB under AC electric field while, simultaneously, electrons are injected into EML from LiF/Al electrode through TmPyPB ETL. The holes and electrons in the EML then form excitons that subsequently emit light upon recombination (left scheme). The reversal of polarity (in the positive field) results in the injection of holes into the device, and these holes drift toward the insulator and neutralize the negative ionized dopants in the Poly-TPD:F4TCNQ HGL (right scheme).

therefore propose a mechanism that the holes can be injected from LiF/Al electrode through TmPyPB as a possible responsibility for refilling the depleted Poly-TPD:F4TCNQ HGL when the polarity of the electric field is reversed, that is, in the positive half of the AC cycle, as shown in Figure 5b (right scheme). This can be proved by the fact that, as shown in Figure S6 (Supporting Information), the device with TmPyPB ETL but without Poly-TPD:F4TCNQ HGL exhibits higher luminance compared to the device without both ETL and HGL. Since no electrons and holes are generated in the two devices, the holes and electrons are originally from the injection from external electrode. Therefore, the operation mechanism of the two devices in Figure S6 (Supporting Information) can be proposed as follow. In the negative half of the AC cycle, electrons are injected into the EML from LiF/Al electrode ETL and accumulated at the interface of P(VDF-TrFE-CFE)/EML. When the AC cycle is positive, holes are also effectively injected into the EML from LiF/Al electrode. Simultaneously, the accumulated electrons move into the EML to form excitons with the injected electrons,

leading to light emission upon recombination. Although it is hard to inject holes from LiF/Al electrode due to the mismatch energy, there is the only source to supply holes in this device, which corresponds to our recent report where we use Ca/Al as the injected electrode.[11] The higher luminance in the device with TmPyPB ETL in comparison to the device without both ETL and HGL in Figure S6 can be attributed to the significant enhancement of electron injection by lowering the injection barrier, and the hole injection cannot be seriously reduced, thus improving the recombination of electrons and holes in AC-driven condition.[11] The operation mechanism of devices in Figure S6 (Supporting Information) strongly demonstrates that both holes and electrons can be injected into our devices from the TmPyPB ETL in AC-driven condition. Furthermore, a hole-only device was employed to investigate the hole injection from LiF/Al electrode through TmPyPB, where the hole current density were achieved up to 1.8 mA $cm^{-2}$ at a DC voltage of 30 V (Supporting Information, Figure S11). Note that there is no light emission from the device in the whole driving voltage, demonstrating no electrons injection. In the high AC voltage in our FIPEL devices (Vrms is up to 100 V), thus the hole current density could be much higher. This strongly demonstrated that the holes can be injected from LiF/Al electrode. Therefore, the injected holes from LiF/Al electrode through TmPyPB are drift towards the insulator and neutralize the negative ionized dopants in the Poly-TPD:F4TCNQ HGL in the positive half of the AC cycle. This brings the system back to the original state. By this process, free charges can be regenerated that are used in the subsequent negative cycle to generate excitons again.

## 3. Conclusions

In summary, we have successfully demonstrated highly efficient solution-processed FIPEL devices with maximum luminance, $\eta_{cd}$, and $\eta_p$ values of 3000 cd $m^{-2}$, 15.8 cd $A^{-1}$, and 3.1 lm $W^{-1}$ for blue emission, 13 800 cd $m^{-2}$, 76.4 cd $A^{-1}$, and 17.1 lm $W^{-1}$ for green emission, and 1600 cd $m^{-2}$, 8.8 cd $A^{-1}$, and 1.8 lm $W^{-1}$ for orange-red emission. The simple multilayer structure between the two electrodes, consisting of a high-*k* dielectric layer, a conjugated polymer hole generation layer, a phosphorescent emissive layer and a high-triplet electron transport layer, was entirely deposited using spin-coating from solutions. Our results demonstrate that high-efficiency FIPEL devices with state-of-the-art performance can be achievable using solution-processed fabrication. The high luminance and efficiency can be further expected if using thin dielectric layer with high dielectric constant. This unprecedented performance enabled the low-cost mass production of FIPEL devices using roll-to-roll processing for next-generation displays and solid-state lighting.

## 4. Experimental Section

*Materials*: The high-*k* relaxor ferroelectric terpolymer dielectrics, poly(vinylidene fluoride-trifluoroethylene-chlorofluoroethylene) [P(VDF-TrFE-CFE)], Poly(*N,N'*-bis(4-butylphenyl)-*N,N'*-bis(phenyl) benzidine) (Poly-TPD), and poly (*N*-vinylcarbazole) (PVK) were purchased from PiezoTech, American Dye Source, and Sigma-Aldrich, respectively. Tetrafluoro-tetracyano-quinodimethane (F4TCNQ), 1,3-bis(2-(4-*tert*-butylphenyl)-1,3,4-oxadiazo-5-yl)benzene (OXD-7), bis(3,5-difluoro-2-(2-pyridyl) phenyl-(2-carboxypyridyl)iridium (FIrpic), fac-tris(2-phenylpyri-dine)iridium(III) [Ir(ppy)$_3$], bis(2-methyldibenzo[f,h] quinoxaline) (acetylacetonate) iridium (III) [Ir(MDQ)$_2$(acac)], 1,3,5-tri(m-pyrid-3-yl-phenyl)benzene (TmPyPB) were purchased from Luminescence Technology Corp., Taiwan, All materials are used as received without further purification.

*Device Fabrication*: All FIPEL devices were fabricated on a glass substrate with a pre-coated ITO film 100 nm thick, with a sheet resistance of approximately 10 Ω/□. First, the substrates were cleaned in an ultrasonic bath with acetone followed by methanol and isopropanol for 30 min each. The ITO substrates subsequently were dried in a vacuum oven for 2h and treated with UV-ozone for 20 min. The dielectric layers were made by spin coating 100 mg $mL^{-1}$ P(VDF-TrFE-CFE) solutions in dimethylformamide (DMF) on top of ITO at 1500 rpm inside a nitrogen filled glove box with low moisture and oxygen content (<0.1 ppm), followed by thermal annealing at 135 °C for 4 h. The Poly-TPD doped 7% F4TCNQ as the hole generation layer was spin-coated using 12 mg $mL^{-1}$ in chlorobenzene at 3000 rpm, followed by baking at 120 °C for 30 min. The EML consisted of a blend of PVK and OXD-7 (PVK:OXD-7 = 80:20, wt/wt) as a co-host and 10 wt% phosphors as the dopant. The polymer EML was obtained by spin coating of the 18 mg $mL^{-1}$ PVK:OXD-7:phosphors blend in chlorobenzene onto the Poly-TPD:F4TCNQ layer at 2000 rpm and dried at 120 °C for 30 min. A 24 mg $ml^{-1}$ small-molecule electron-transport material TmPyPB was dissolved in formic acid:water (FA:$H_2O$ = 3:1) mixture as previously reported[19] and spun cast onto the EML at a spin speed of 4000 rpm followed by drying at 80 °C for 30 min. Device fabrication was completed by thermal evaporation of LiF (1 nm)/Al (100 nm) electrode through a shadow mask under vacuum at a base pressure of ≈ $5 \times 10^{-6}$ Torr at a rate of 0.05 nm $s^{-1}$. The overlap between ITO and Al electrodes was 3 mm×3 mm as the active emissive area of the devices. Capacitors consisting of the P(VDFTrFE-CFE) terpolymer dielectric with Al electrodes were fabricated for the measurement of the dielectric properties. The Al bottom electrodes of the capacitors were thermally evaporated onto the glass substrates through a shadow mask. Then 100 mg $mL^{-1}$ P(VDFTrFE-CFE) terpolymer solution was spin-coated onto the substrates at 1500 rpm followed by thermal annealing at 135 °C for 4 h in a glovebox. Finally, the top Al electrodes were deposited by evaporation through a shadow mask. The effective area of each device is 9 $mm^{-2}$.

*Electrical, Optical, and Microscopic Characterization of Thin Films*: The thickness of the films were measured by a calibrated Dektak 6M profiler (Veeco). Capacitance-voltage characteristics were measured with a Keithley 595 quasistatic *CV* meter. The dielectric constant was calculated from the capacitance. The DC current-voltage characteristics hole-only devices and FIPEL devices were measured by using a Keithley source measurement unit (Keithley 236). The photoluminescence (PL) spectra were recorded on a Hitachi F-4500 fluorescence spectrophotometer. The atomic force microscopy (AFM) topography image was done with a nanoManipulator (3rd Tech, Chapel Hill, North Carolina).The cross-sectional scanning electron microscope (SEM) image was observed using a field-emission (FESEM) (JEOL JSM-6330F). For thin-film X-Ray Diffraction, thin films were fabricated under identical conditions with the FIPELs. XRD data were collected on a Bruker D8 Discover with DaVinci diffractometer, in the standard Bragg-Brentano para-focusing configuration utilizing sealed tube CuKã radiation and operated at 40 kV and 40 mA. The sample was mounted on a horizontal sample stage on a 830 mm diameter goniometer equipped with a 1D Lynxeye detector. Data were collected using a step width of 0.013° and step time of 0.2 s with a 2$\theta$ range of 3.0°–40.0°. The Bruker Diffrac. Suite Measurement and EVA software packages were used for data collection and processing. All measurements were carried out under ambient conditions at atmospheric pressure and room temperature.

*Electrical Characterization of Solution-Processed FIPEL Devices*: The AC sinusoidal voltages were applied from a 200 MHz function/arbitrary waveform generator (Agilent 33220A) connected to a Model PZD700A M/S amplifier (Trek) and the voltage was measured on an oscilloscope (Tektronix). The EL spectra were collected with an ILT 950

spectroradiometer (InternationalLight Technologies). The luminance was recorded with an ILT 1400-A photometer (International Light Technologies), as a function of either the AC voltages applied to the devices (at a fixed frequency) or as a function of the frequency of the applied AC voltages (keeping the applied AC bias constant). The time resolved AC electroluminescence response is detected using a fast photo diode. The power input to the device is calculated by measuring the voltage drop across the device and a series resistor (100 Ω) and the phase angle between the two signals using a single phase precision power meter. Capacitance-voltage and phase characteristics were measured with a Keithley 595 quasistatic *CV* meter. All measurements were carried out under ambient conditions at atmospheric pressure and room temperature.

## Supporting Information

Supporting Information is available from the Wiley Online Library or from the author.

## Acknowledgements

The authors would like to thank W. Li and M. Guthold (Wake Forest University, Physics), for atomic force microscopy topography test, and J. Grim, K. Burak, and R. Williams (Wake Forest University, Physics) for photoluminescence spectra test.

Received: July 31, 2013
Revised: September 3, 2013
Published online: October 25, 2013

[1] C. W. Tang, S. A. Vanslyke, *Appl. Phys. Lett.* **1987**, *51*, 913.
[2] T. Tsutsui, S. B. Lee, K. Fujita, *Appl. Phys. Lett.* **2004**, *85*, 2382.
[3] J. Bruckner, N. Christ, O. Bauder, C. Gärtner, M. Seyfried, F. Glöckler, U. Lemmer, M. Gerken, *Appl. Phys. Lett.* **2010**, *96*, 041107.
[4] J. Sung, Y. S. Choi, S. J. Kang, S. H. Cho, T.-W. Lee, C. Park, *Nano Lett.* **2011**, *11*, 966.
[5] A. Perumal, M. Fröbel, S. Gorantla, T. Gemming, B. Lüssem, J. Eckert, K. Leo, *Adv. Funct. Mater.* **2012**, *22*, 210.
[6] A. Perumal, B. Lussem, K. Leo, *Appl. Phys. Lett.* **2012**, *100*, 103307.
[7] A. Perumal, B. Lussem, K. Leo, *Org. Electron.* **2012**, *13*, 1589.
[8] S. H. Cho, J. Sung, I. Hwang, R. H. Kim, Y. S. Choi, S. S. Jo, T. W. Lee, C. Park, *Adv. Mater.* **2012**, *24*, 4540.
[9] Y. H. Chen, G. M. Smith, E. Loughman, Y. Li, W. Y. Nie, D. L. Carroll, *Org. Electron.* **2013**, *14*, 8.
[10] Y. H. Chen, Y. D. Xia, Y. Gu, C. L. Yang, G. M. Smith, D. L. Carroll, *Appl. Phys. Lett.* **2013**, *102*, 013307.
[11] Y. D. Xia, Y. H. Chen, G. M. Smith, Y. Li, W. X. Huang, D. L. Carroll, *Appl. Phys. Lett.* **2013**, *102*, 253302.
[12] R. P. Ortiz, A. Facchetti, T. J. Marks, *Chem. Rev.* **2010**, *110*, 205.
[13] Q. M. Zhang, V. Bharti, X. Zhao, *Science* **1998**, *280*, 2101.
[14] T. C. Chung, A. Petchsuk, *Macromolecules* **2002**, *35*, 7678.
[15] X. Chen, L. Liu, S. Z. Liu, Y. S. Cui, X. Z. Chen, H. X. Ge, Q. D. Shen, *Appl. Phys. Lett.* **2013**, *102*, 063103.
[16] J. H. Li, Z. H. Sun, F. Yan, *Adv. Mater.* **2012**, *24*, 88.
[17] L. Qian, Y. Zheng, J. G. Xue, P. H. Holloway, *Nat. Photonics* **2011**, *5*, 543.
[18] K. H. Yim, G. L. Whiting, C. E. Murphy, J. J. M. Halls, J. H. Burroughes, R. H. Friend, J.-S. Kim, *Adv. Mater.* **2008**, *20*, 3319.
[19] T. Earmme, S. A. Jenekhe, *Adv. Funct. Mater.* **2012**, *22*, 5126.
[20] S. H. Zhang, N. Y. Zhang, C. Huang, K. L. Ren, Q. M. Zhang, *Adv. Mater.* **2005**, *17*, 1897.
[21] N. Levi, R. Czerw, S. Y. Xing, P. Iyer, D. L. Carroll, *Nano Lett.* **2004**, *4*, 1267.
[22] Q. M. Zhang, V. Bharti, X. Zhao, *Science* **1998**, *280*, 2101.
[23] S. J. Su, T. Chiba, T. Takeda, J. Kido, *Adv. Mater.* **2008**, *20*, 2125.
[24] X. H. Yang, D. C. Muller, D. Neher, K. Meerholz, *Adv. Mater.* **2006**, *18*, 948.
[25] D. Kabra, L. P. Lu, M. H. Song, H. J. Snaith, R. H. Friend, *Adv. Mater.* **2010**, *22*, 3194.
[26] S. L. Gong, Y. H. Chen, X. Zhang, P. J. Cai, C. Zhong, D. G. Ma, J. G. Qin, C. L. Yang, *J. Mater. Chem.* **2011**, *21*, 11197.
[27] Z. Q. Jiang, Y. H. Chen, C. Fan, C. L. Yang, Q. Wang, Y. T. Tao, Z. Q. Zhang, J. G. Qin, D. G. Ma, *Chem. Commun.* **2009**, 3398.
[28] C. M. Han, Z. S. Zhang, H. Xu, S. Z. Yue, J. Li, P. R. Yan, Z. P. Deng, Y. Zhao, P. F. Yan, S. Y. Liu, *J. Am. Chem. Soc.* **2012**, *134*, 19179.
[29] M. C. Gwinner, D. Kabra, M. Roberts, T. J. K. Brenner, B. H. Wallikewitz, C. R. McNeill, R. H. Friend, H. Sirringhaus, *Adv. Mater.* **2012**, *24*, 2728.
[30] Q. Wang, J. Q. Ding, D. G. Ma, Y. X. Cheng, L. X. Wang, X. B. Jing, F. S. Wang, *Adv. Funct. Mater.* **2009**, *19*, 84.
[31] Q. Wang, J. Q. Ding, D. G. Ma, Y. X. Cheng, L. X. Wang, F. S. Wang, *Adv. Mater.* **2009**, *21*, 2397.